Self-Assembled Architectures with Segregated Donor and Acceptor Units of a Dyad Based on a Monopyrrolo-Annulated TTF–PTM Radical

Self-assembled architectures with segregated donor and acceptor units of a dyad based on a monopyrrolo-annulated TTF-PTM radical

Manuel Souto,[a] Marta V. Solano,[b] Imma Ratera,[a] Morten Jensen,[b] Dan Bendixen,[b] Francesca Delchiaro,[c] Alberto Girlando,[c] Anna Painelli,[c] Jan O. Jeppesen,[b] Concepció Rovira,[a] and Jaume Veciana*[a]

Abstract: An electron donor-acceptor dyad based on a polychlorotriphenylmethyl (PTM) radical subunit linked to a tetrathiafulvalene (TTF) unit through a π-conjugated *N*-phenyl-pyrrole-vinylene bridge has been synthesized and characterized. The intramolecular electron transfer (IET) process and magnetic properties of the radical dyad have been evaluated by cyclic voltammetry, UV-Vis, vibrational, and ESR spectroscopies both in solution and in the solid state. The self-assembling ability of the radical dyad and of its protonated non-radical analogue has been investigated by X-ray crystallographic analysis which reveals that the radical dyad produces a supramolecular architecture with segregated donor and acceptor units where the TTF subunits are arranged in 1-D herringbone type stacks. Analysis of the X-ray data at different temperatures suggests that the two non-equivalent molecules that form the asymmetric unit of the crystal of the radical dyad evolve into an opposite degree of electronic delocalization as the temperature decrease.

Introduction

Molecules that can be switched between two or more states through the application of an external stimulus (i.e., temperature or light) have attracted a great deal of attention for application in information technology.[1-6] Organic molecules which contain electron donor (D) and electron acceptor (A) units linked by π-conjugated bridging groups (D-π-A dyads) are of interest in this respect on account of the presence of intramolecular electron transfer (IET) processes.[7-11] Some of us have been focused on the study of bistability of several D-A systems made of polychlorotriphenylmethyl (PTM) radicals, as electron acceptors, and ferrocene (Fc) derivatives, as electron donor units. These systems can be switched through an IET from the neutral (N) to the zwitterionic (Z) state by changing the polarity of the surrounding medium and in solvents of intermediate polarity both states can coexist simultaneously.[12-18]

Tetrathiafulvalene (TTF) and its derivatives have been frequently used as donor units in D-A ensembles that are of prime interest on account of their potential applications in electronic and optoelectronic devices.[19-26] More interesting are TTF-based dyads that exhibit molecular packings with a complete segregation of the donor and acceptor fragments forming homo-stacks of TTF subunits. Segregated stacks are in fact a prerequisite for obtaining conducting materials.[27-29] In addition, systems with segregated TTF subunits may bring the opportunity to study the interplay in the solid state between the bistability associated with IET and the intermolecular charge transfer (CT) phenomena typically related with stacks of neutral and/or charged TTF molecules of conducting solids. With this objective in mind, some of us have recently reported a D-A system **1**, which was based on a TTF electron π-donor connected to the PTM electron acceptor by a vinylene bridge (Scheme 1).[30] This radical dyad exists in solution in equilibrium with the homo- and the mixed-valence dimers under the influence of concentration, polarity of the solvent,[30,31] and temperature.[32,33] The appearance of both kinds of aggregates is governed by the reciprocal influence of the IET within the dyad and the intermolecular CT occurring in the dimers between the TTF subunits. Unfortunately, up to date, it has not been possible to study in detail the interplay between the IET and CT in the solid state and its relationship with the molecular packing because of the poor crystalline quality of radical dyad **1** that prevented the determination of its X-ray crystal structure.

[a] M. Souto, Dr. I. Ratera, Prof. C. Rovira, Prof. J. Veciana
Department of Molecular Nanoscience and Organic Materials
Institut de Ciència de Materials de Barcelona (ICMAB-CSIC)/CIBER-BBN
Campus Universitari de Bellaterra, 08193 (Barcelona), Spain
E-mail: jveciana@icmab.es

[b] Dr. M. V. Solano, M. Jensen, D. Bendixen, Prof. J. O. Jeppesen
Department of Physics, Chemistry and Pharmacy
University of Southern Denmark
5230 Odense M, Denmark

[c] F. Delchiaro, Prof. A. Girlando, Prof. A. Painelli
Dipartamento di Chimica
Parma University/INSTM-UdR Parma
I-43124 Parma, Italy

Supporting information for this article is given via a link at the end of the document.

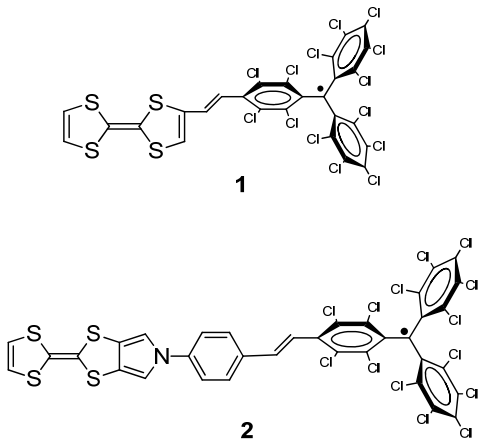

Scheme 1. Molecular structures of radical D-A dyads **1** and **2**.

In order to improve the self-assembly of the TTF moieties of TTF-PTM dyads and their crystalline quality, we have designed a new TTF-based radical dyad **2** (Scheme 1) with a longer bridge between the TTF and PTM units. The increased length of the bridge was obtained using a monopyrrolo-TTF (MPTTF) building block allowing a conjugated *N*-phenyl-pyrrole-vinylene ring to be annulated directly to the TTF moiety.

Herein, we report the synthesis of the new donor-acceptor system based on the MPTTF-PTM radical dyad **2** followed by its characterization carried out using a variety of techniques including cyclic voltammetry (CV), UV-Vis, Raman, and ESR spectroscopies as well as theoretical calculations. These studies reveal that the MPTTF-PTM radical dyad **2** exists in its neutral radical form both in the solid state and in solution rather that in a zwitterionic form. Furthermore, X-ray analysis of dyad **2** revealed an interesting self-assembly architecture with segregated donor and acceptor units that have been analyzed in detail using a variety of techniques. Finally, analysis of bond lengths reveals opposite changes in the degree of delocalization for the two non-equivalent molecules constituting the crystallographic asymmetric unit when the temperature was decreased.

Results and Discussion

Synthesis: Initially, we describe an improved synthesis of the MPTTF derivative[34] **6** before outlining the synthesis of the novel MPTTF-PTM dyad **2**. The synthesis of the MPTTF derivative **6** was carried out as outlined in Scheme 2. Cross-coupling of 1,3-dithiole-2-thione (**3**) and 5-tosyl-(1,3)-dithiolo[4,5-*c*]pyrrole-2-one[35,36] (**4**) in neat $(EtO)_3P$ gave **5** in 71% yield after column chromatography.

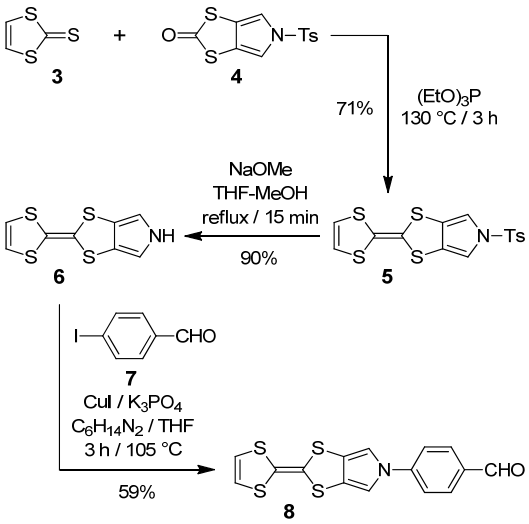

Scheme 2. Synthesis of the *N*-(4-formylphenyl)-MPPTF derivative **8**.

The tosyl protecting group on the MPTTF derivative **5** was removed by using NaOMe in a THF/MeOH mixture producing compound **6** in 90% yield, which subsequently was subjected to a modified Buchwald-Hartwig reaction.[37-39] Thus, by mixing compound **6**, 4-iodobenzaldehyde (**7**), an excess of cuprous iodide (CuI), and *trans*-1,2-diaminocyclohexane ($C_6H_{14}N_2$), the *N*-(4-formylphenyl)-MPPTF derivative **8** was obtained (Scheme 2) in 59% yield after purification by column chromatography.

The three-step synthesis of the MPTTF-phenyl-PTM radical **2** is summarized in Scheme 3. Compound **10** was obtained in 69% yield through a Horner-Wadsworth-Emmons reaction of compound **8** and the protonated PTM derivative **9** functionalized with a phosphonate group, whose synthesis has been reported elsewhere.[40] A subsequent deprotonation of **10** with tetrabutylammonium hydroxide (TBAOH) followed by oxidation of the formed carbanion with silver nitrate ($AgNO_3$) afforded the radical dyad **2** (71%) as a black solid, which is stable under atmospheric conditions (Scheme 3).

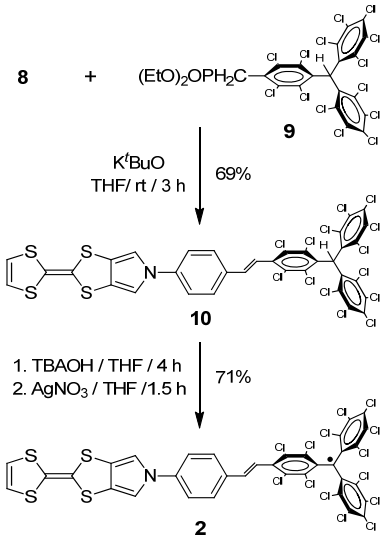

Scheme 3. Synthesis of the MPTTF-Phenyl-PTM radical **2**.

Electrochemical properties: The electrochemical properties were studied by means of CV. Cyclic voltammograms (CVs) of compounds **1**, **2** (Figure 1), and **10** (Figure S2) were recorded in CH_2Cl_2 at room temperature. Compound **10** exhibit two quasi reversible redox waves which can be assigned to the stepwise oxidation of the MPTTF moiety to $MPTTF^{+}\cdot$ and $MPTTF^{2+}$ with redox potentials of +0.49 and +0.99 V (vs. Ag/AgCl), respectively. As expected, the CV of radical **2** exhibits three waves, related to the following redox pairs: $PTM^{-}/PTM\cdot$, $MPTTF/MPTTF^{+}\cdot$, and $MPTTF^{+}\cdot/MPTTF^{2+}$, at redox potentials of −0.19, +0.45, and +0.95 V (vs. Ag/AgCl), respectively (Scheme S7). Oxidation potentials of the MPTTF subunits of compounds **2** and **10** show positive shifts compared to the unsubstituted MPTTF **6** (+0.37 and +0.72 V)[34] obtained under the same conditions, consistent with the presence of electron withdrawing chlorinated aromatic fragments in compounds **2** and **10**. In addition, the oxidation potentials shift toward more positive values for **1** when compared to **2**, an observation which most likely can be accounted for by the lower interaction taking place between the D and A subunits in **2** because of the increased length of the bridge connecting the D and A subunits.

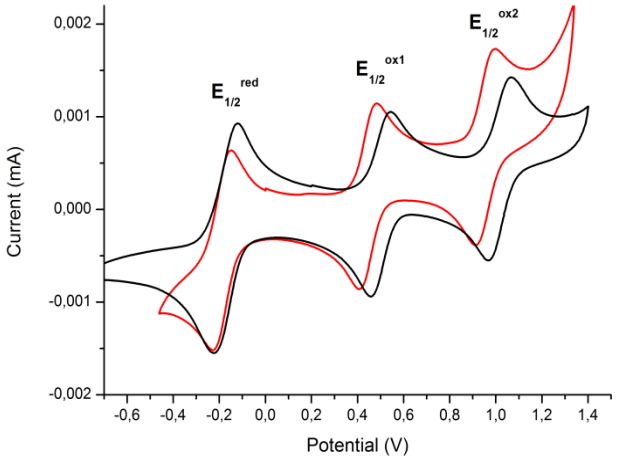

Figure 1. Cyclic voltammograms (CVs) of compounds **1** (black line) and **2** (red line) (0.05 mM) in CH_2Cl_2 vs. Ag/AgCl using *n*-Bu_4PF_6 (0.1 M) as electrolyte at 300 K under argon at a scan rate of 0.1 V s^{-1}.

Optical properties: The UV-Vis-NIR spectrum (Figure 2) of dyad **2** recorded in THF at 300 K shows an intense absorption band at 385 nm, characteristic of PTM radical chromophores, with a shoulder at 376 nm which can be attributed to the MPTT fragment. The two unresolved peaks appearing at lower energies at 439 and 550 nm, respectively, can be assigned to the electronic conjugation of the unpaired electron into the □-framework. Interestingly, the radical dyad **2** also shows a weak and broad absorption band around 800 nm which can be ascribed to the IET taking place between the TTF donor and the PTM acceptor, whereas a similar IET band is observed in the region between 900-1000 nm for the shorter radical dyad **1**.[41] The hypsocromic shift observed in **2**, as compared to **1**, can be ascribed to the lower donor character of the MPTTF subunit.

When dyad **2** was oxidized with one equivalent of $Fe(ClO_4)_3$, the IET absorption band disappears and a new band appears around 600 nm, which most likely can be assigned to the formation of the radical-cation of the MPTTF subunit. (Figure S3).

In order to compare the bistability in solution of dyads **1** and **2**, the UV-Vis-NIR spectra of **2** were recorded in different solvents (see Figure S4).[30] Its was realized that the bistability of dyad **2** was only observed in the highest polar solvent assayed, e.g., DMF, as demonstrated by the appearance of a band at 512 nm with a small intensity attributed to the presence of a small percentage of dyad **2** in the zwitterionic state, coexisting with the neutral state in the polar DMF medium. This observation is in deep contrast with the behavior of dyad **1**. In DMF, **1** exists only in the

zwitterionic state and even in medium polarity solvents, such as acetone and CH_2Cl_2/acetone mixtures **1** was found to exist in the zwitterionic state. This remarkable difference can in part be ascribed to the poorer electron donor character of the MPTTF unit in comparison with the TTF unit. We observe, however, that the formation of zwitterionic species of **1** dissolved in medium and high polarity solvents is actually triggered by the formation of $(TTF^{+})_2$ and mixed-valence dimers. Possibly, attaching the pyrrole ring to the TTF moiety reduces the well-known tendency of TTF to form dimers, thus hindering the formation of zwitterionic species.

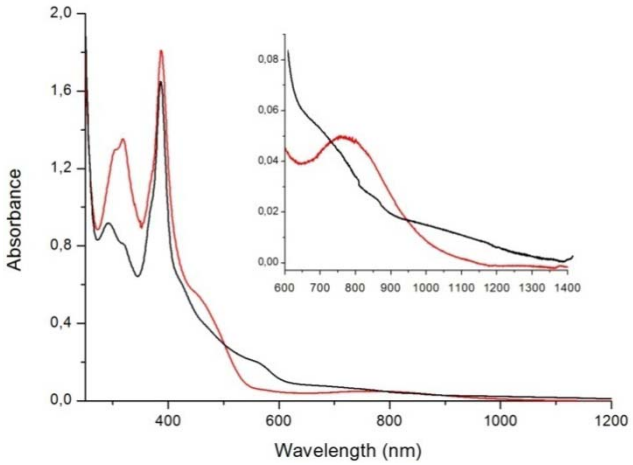

Figure 2. UV-Vis-NIR spectra recorded in THF at 300 K of a 0.05 mM solution of dyads **1** (black line) and **2** (red line). The inset shows the low-energy range of the absorption spectra of **1** and **2**.

Magnetic properties: The ESR spectrum (Figure 3) of **2** recorded in CH_2Cl_2 (0.05 mM) at 300 K shows, centered at a *g*-value of 2.0029, two partially overlapped main lines corresponding to the coupling of the unpaired electron with one ^{1}H atom of the vinylene spacer along with a few weak satellite lines because of the coupling with naturally abundant ^{13}C isotopes at the □- and aromatic positions. The isotropic hyperfine coupling constants with such nuclei show the usual values for vinylene substituted PTM radicals; i.e., $a_1(H)$=1.99 G, $a_{13}(C_{□□}$=30.0 G, $a_{13}(C_{o,p})$=12.5 G.

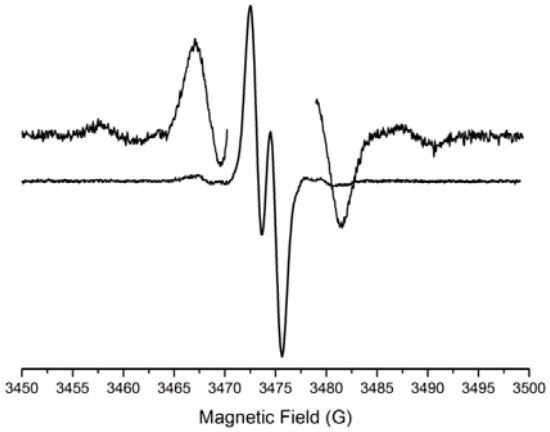

Figure 3. ESR spectrum of a 0.05 mM solution of dyad **2** recorded in CH_2Cl_2 at 300 K.

The ESR spectrum of **2** recorded in the crystalline state at 120 K consists on an asymmetric line indicative of an axial symmetry with g_a = 2.0045 and $g_b = g_c$ = 2.0027 (Figure S5). Moreover, the ESR lineshape of **2** does not exhibit any significant change in the temperature range of 120-320 K, with its intensity following the Curie law; as for dyad **1** (Figures S6-S7). These results suggest there is no bistability in the solid state associated with an IET for either radical dyad **1** or **2**. Indeed, in the presence of bistability one would expect large changes in the position and shape of the EPR line, due to the large differences of the magnetic anisotropies of PTM radicals and TTF/MPTTF cation-radicals.

Crystal structure of compound 10: X-ray diffraction analysis at 300 K on red crystals of **10**, obtained by slow evaporation from a solution of Et_2O/CH_2Cl_2, indicates it crystallizes in the triclinic system with a P-1 space group (Figure S8 and Tables S1 and S2). The molecular structure of **10** (Figure 4) shows that the vinylene bridge is coplanar with the phenyl ring and it has a *trans*-configuration. The asymmetric unit is formed by two non-equivalent molecules (**10A** and **10B**) in a *head-to-tail* arrangement (Figure 5). The phenyl and pyrrole rings are not coplanar, showing torsion angles C14-C9-N1-C4 of *ca.* 26 and 23º for **10A** and **10B**, respectively. Moreover, the MPTTF unit is somewhat distorted in the typical boat conformation with a torsion angle S3-C6-S4-C8 of *ca.* 14º and the average of MPTTF C=C bond lengths is 1.34 Å for **10A** and 1.43 Å for **10B**. The MPTTF moieties of neighboring molecules are forming alternated *face-to-face* dimers of **10A**···**10A** or **10B**···**10B** molecules on the *bc* plane forming 1-D chains along the *c*-axis with shortest S-S distances of 3.92 and 3.98Å, respectively

(See Figure 5 and Table S3). On the other hand, the PTM units are also stacked forming monodimensional chains along the c-axis with short intermolecular Cl···Cl interactions that are in the range of 3.28-3.47 Å (Figure S10).

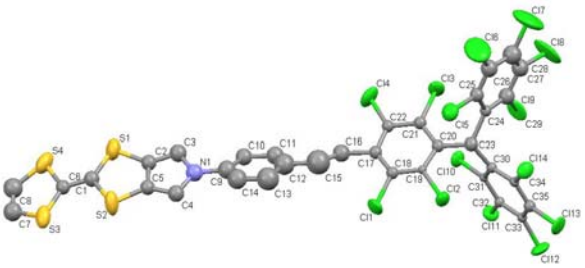

Figure 4. ORTEP views of compound **10** at 300 K. Hydrogen atoms have been omitted for clarity.

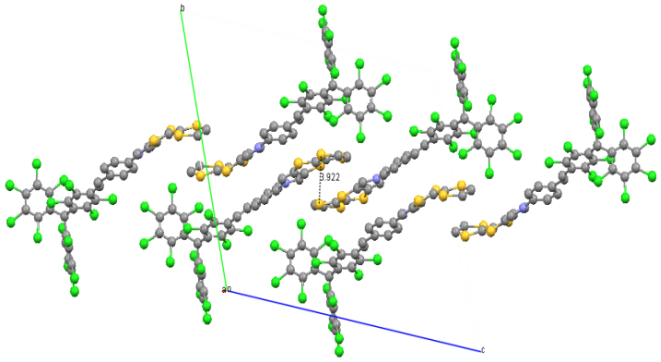

Figure 5. Molecular packing of compound **10** at 300 K in the *bc* plane.

Crystal structure of compound 2: X-ray diffraction analysis at 150 and 300 K on small black crystals of radical dyad **2**, obtained by a slow evaporation from a *n*-hexane/CH_2Cl_2 solution, indicates it crystallizes in the monoclinic system with the space group P21 (Figure 6 and Tables S1 and S2). The asymmetric unit reveals two non-equivalent molecules (**2A** and **2B**) that are aligned in parallel along the *a*-axis as shown in Figure S12. The molecular structure of **2** is alike to that of **10** since it shows that the vinylene bridge is coplanar with the phenyl ring with a *trans*-configuration and with the phenyl and pyrrole rings twisted with a torsion angle C14-C9-N1-C4 of *ca.* 31º. The MPTTF subunits are also distorted with a torsion angle S3-C6-S4-C8 of *ca.* 10º and with central C=C bond lengths of 1.36 Å, demonstrating that the TTF is still in the neutral state[42] (but with certain degree of charge delocalization over the conjugated skeleton). The main differences between the non-radical compound **10** and the radical dyad **2** are located on the vinylene bridge and the PTM region. In fact, the vinylene-bridge region of **2** exhibits a higher degree of electron delocalization than **10** as estimated by calculating the differences between the single C-C bonds and C=C double bonds lengths. These difference values pass from 0.33-0.35 Å for **10A** and **10B** to 0.17 Å for **2A** and **2B** at 300 K demonstrating that the PTM radical unit in dyad **2** induces a higher electron-withdrawing effect over the rest of the molecule in contrast with what is observed in compound **10**. On the other hand, the average of the distance between the central C23 atom of PTM and C20, C24 and C30 atoms is *ca.* 1.54 Å in **10** and 1.46 Å in **2**, showing a partial double-bond character in **2** that indicates a weak delocalization of the unpaired electron into the aromatic rings, as reported for other PTM derivatives.[43]

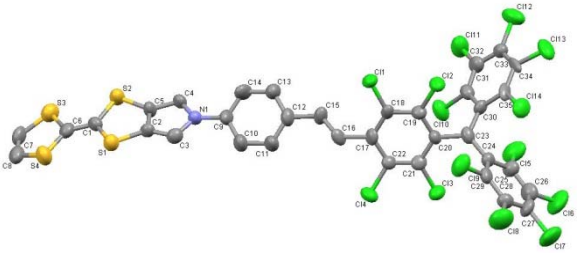

Figure 6. ORTEP views of radical dyad **2** at 300 K. Hydrogen atoms have been omitted for clarity.

Molecules of radical dyad **2** are arranged as shown in Figure 7 forming regular 1-D chains of equivalent molecules (**2A** or **2B**) where the MPTTF subunits form a *herringbone* structure along the *b*-axis with short Cl···Cl contacts in the range of 3.30-3.49 Å and S···S short contacts of 3.95 Å and 3.90 Å for **2A** and **2B**, respectively (See Table S3). However, this supramolecular assembly is different over the *a*-axis, where there is no overlap between the S atoms and the stacking is governed by S···Cl and S···C(pyrrole) interactions of 3.52 Å and 3.45 Å, respectively, alternating molecules of **2A** and **2B** (Figures 8 and S14)

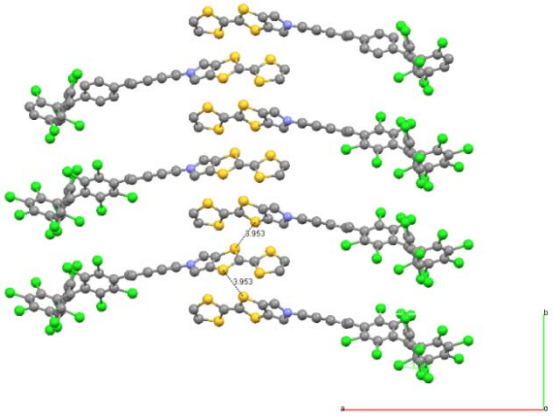

Figure 7. Molecular packing of **2A** molecules at 300 K in the *ab* plane.

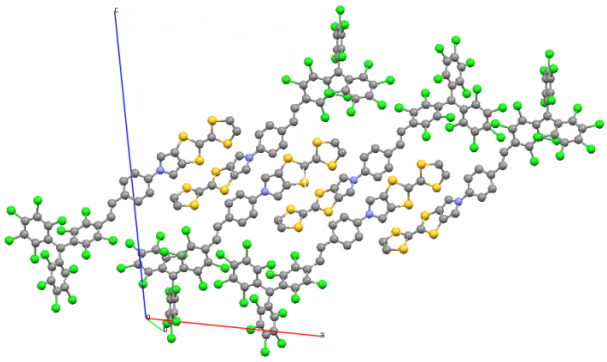

Figure 8. Molecular packing of radical dyad **2** at 300 K in the *ac* plane.

In order to study possible changes in the molecular structure at low temperatures, the X-ray crystal structure of radical dyad **2** was obtained at 150 K (See Tables S1 and S2). Interestingly, the degree of delocalization of the two non-equivalent molecules (**2A** and **2B**) of dyad **2**, that is very similar at room temperature, changes drastically for both molecules in opposite directions at 150 K since molecules **2B** become much more delocalized along their entire skeletons than molecules **2A** at 150 K. Indeed, molecule **2B** at 150 K exhibits a higher degree of delocalization as demonstrated by the shortness of the N1-C9 (1.39 Å for **2B** and 1.45 for **2A**), the difference between the single C-C bonds and C=C double bonds in the vinylene-bridge region which are 0.21 for **2A** and 0.09 for **2B**, as well as the difference C-S – C=C in the MPTTF region which are 0.45 for **2A** and 0.37 for **2B**. This interesting observation could be because of the different surrounding polar environment that involves the two different molecules (**2A** and **2B**) that possibly modifies the electrostatic interactions between molecules by the surrounding media. It is important to be note that molecule **2A** has three nearby Cl atoms surrounding the MPTTF unit, whereas molecule **2B** has only two Cl atoms near to the MPTTF unit as shown in Figure S13. On the other hand, decreasing the temperature to 150 K, the intermolecular S···S short distances between neighboring molecules inside the stacks formed by **2A** or **2B** molecules along the *b*-axis also decrease up to 3.89 and 3.85 Å, respectively (Figure S15).

The structural changes observed at low temperatures suggested that modifications in the electronic structures may occur. To evaluate these modifications, hopping integrals between the MPTTF units in neighboring MPTTF-PTM moieties were calculated on the basis of the ZINDO method.[44] The hopping integrals for the structure at 300 K along the *b*-axis (Figure 7) were found to be 12 meV and 20 meV between molecules **2A**···**2A** and **2B**···**2B**, respectively, and 10 meV for the dimer **2A**···**2B** along the *a*-axis (Figure 8). Interestingly, at a lower temperature (150 K) the hopping integral of **2A**···**2A** increases to 19 meV whereas the integral between **2B**···**2B** decreases down to 1 meV. Therefore, whereas the hopping integral of **2A**···**2A** increases by lowering *T*, as expected in consequence of lattice contraction, that between **2B**···**2B** essentially disappears making the **2B** units practically isolated within the stack.

Polarized IR-NIR-Visible and Raman Spectra in the Solid State: The polarized IR and NIR-visible absorption spectra (Figure 9) recorded of the dyad **2**, shows the low frequency electronic transitions. The spectrum, with electric vector parallel to the crystal *b* axis (red line), is limited to 11000 cm^{-1} because beyond this frequency the spectrum is completely saturated. A band around 8900 cm^{-1} (1120 nm) is clearly discernible. The origin of this band is unclear at present stage. It is unlikely that it is associated with intermolecular CT (ICT), since the MPTTF units are essentially neutral (*vide infra*). The spectrum with electric vector perpendicular to the *b* axis (black line), namely, approximately along the direction of ICT transition dipole moment, shows two bands before reaching saturation around 18000 cm^{-1}, one at about 10500 cm^{-1} (950 nm) and the other at about 15200 cm^{-1} (660 nm). The latter might be the solid state counterpart of the band observed in solution around 700 nm, and attributed to IET. Both the 10500 cm^{-1} and the 15200 cm^{-1} bands, which are very weak, have a polarization compatible with IET.

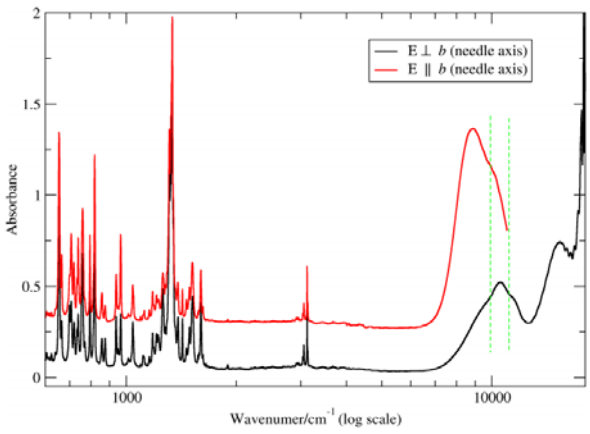

Figure 9. Extended polarized absorption spectra of a crystal of dyad **2** with logarithmic scale for the

frequencies. The dashed green lines mark the points of beam splitter/detector changes.

The Raman spectrum of dyads **1** and **2** were recorded at 300 K using an excitation wavelength of 1064 nm in the near IR region (Figure S16). The Raman bands close to 1600 cm^{-1} are attributed to the C=C stretching mode of the vinylene spacer whereas the bands around 1510 cm^{-1} are characteristic for the stretching mode of the lateral polychlorinated benzene groups.[45] This Raman band shifts toward higher frequencies when there is an increment of effective □-electron delocalization into the PTM subunit. This Raman shift is well observed in the spectrum of the oxidized derivative $\mathbf{1}^{+\cdot}$ where there is a downshift from 1515 to 1508 cm^{-1},[32] due to the suppression of the IET process because of the lack of the donor character of the oxidized TTF subunit. Comparing the spectra of **1** and **2**, it can be stated that there is a higher electron (and spin) delocalization in compound **1** as demonstrated by its higher Raman shift. Moreover, it is well known that vibrational spectroscopy can provide a reliable estimate of the formal charge or degree of CT on the molecular sites.[46] In the case of TTF, the charge sensitive vibrations are associated with the C=C stretching, notably the Raman active $□_3$ mode, which appears at 1516 in neutral TTF and at 1420 cm^{-1} in the radical-cations, and the infrared active $□_{14}$ mode, respectively found at 1530 and 1478 cm^{-1}.[47-49] The Raman and the IR polarized spectra of **2** (Figure S17) lead us to conclude that the MPTTF C=C stretching overlaps around 1518 cm^{-1} with the above mentioned C=C stretching mode associated with PTM. In this complex situation, it is difficult to obtain a precise estimate of the ionicity, but in any case it can be concluded that in the solid state the TTF/MPTTF subunits of both **1** and **2** dyads are in a practically neutral state.

In order to evaluate if any temperature effect on the CT from the MPTTF to the PTM in the crystals of dyad **2** is present**,** as was observed with the increase of delocalization in the **2B** unit, the Raman spectra of **2** was also recorded at 120 K, in this case, with 752 nm excitation. (Figure S17). In the relevant spectral region we do not observe any downshift on the Raman bands, indicating that there is no CT from the TTF or if present, it is so small that it cannot be detected by means of Raman spectroscopy.

Theoretical calculations: To deepen the understanding the electronic structures of TTF/MPTTF-PTM dyads, a series of quantum chemical calculations have been performed on dyads **1** and **2** in solution, using Gaussian 09 package.[50] Geometries were optimized at (U)CAM-B3LYP/6-31G* level for different oxidation states of **1** and **2** (see Figure S19), the neutral open-shell doublet states (neutral species), the closed-shell anions (anionic species), the cation-biradical (cationic species), where the bi-radicaloid character was enforced by considering the triplet state, and the dication-radical (dicationic species). In all cases, solvent was introduced based on the polarizable continuum model (PCM).[51]

The charge distribution for the neutral radical dyads **1** and **2** (Figure S18) supports a very small degree of CT in the molecule, in line with spectroscopic results. As described in the SI, we divided the molecule in D and A fragments. The charge on each fragment is of the order of 0.09 (for D) and 0.10 (for D) for **1** and **2** in CH_2Cl_2, respectively, and only marginal variations with solvent polarity were obtained. Charge distributions in the cationic, dicationic and anionic species (Figure S18) confirms the CV data, with an excess of electron residing on PTM fragment in the anionic species, and positive charges residing in the TTF/MPTTF fragments in the mono and dicationic species.

The spin distribution in Figure 10 shows that the spin is localized on the PTM moiety and on the vinylene group for the neutral **1** and **2** species, in line with the results obtained using EPR spectroscopy. In the cationic diradicaloid species, the two spin densities on the TTF/MPTTF and PTM units are fully disconnected. As for the ground state charge and spin distributions, the different bridges play a marginal role in affecting the molecular properties.

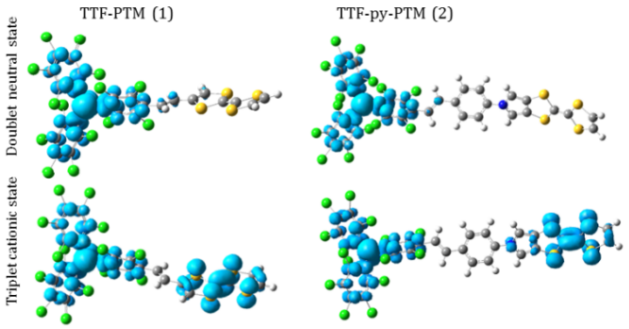

Figure 10. Spin density (light blue) of dyads **1** and **2** in CH_2Cl_2, calculated at UCAMB3LYP/6-31G* level with PCM. Top and bottom panel show results for the neutral and cationic species, respectively. Isovalue of the plot equal to 0.002.

Table 1. Lowest and most intense optical transitions calculated for dyads **1** and **2** in CH_2Cl_2 at TD-UCAM-B3LYP/6-31G* level.

	λ(nm)	oscillator strength	transition nature
1	365	0.10	HOMO-4(β) →SUMO (0.40)
			HOMO-α →LUMO-α (0.21)
	368	0.50	HOMO-4(β) →SUMO (0.18)
			HOMO-β →LUMO-β (0.15)
	375	0.02	HOMO-3(β) → SUMO(0.61)
	474	0.16	HOMO-β →SUMO (0.69)
			HOMO-β →SUMO (0.13)
	636	0.01	HOMO-β → LUMO-β (0.13)
			(HOMO-1)-β → SUMO (0.12)
			(HOMO-1)-β → LUMO-β (0.12)
2	364	0.47	HOMO-5(β) →SUMO (0.11)
			(HOMO-1)α→LUMO-α (0.10)
			(HOMO-3)β→ SUMO (0.11)
			(HOMO-1)β → SUMO (0.21)
	366	0.01	HOMO-6(β) →SUMO (0.81)
	372	0.03	HOMO-5(β) →SUMO (0.71)
	416	0.08	HOMO-β →SUMO (0.76)
	438	0.06	(HOMO-9)-β →SUMO (0.23)
			(HOMO-1)-β → LUMO-β (0.14)
	516	0.013	(HOMO-1)-β → SUMO (0.10)
			(HOMO-3)-β → SUMO (0.07)
			(HOMO-3)-β → LUMO-β (0.07)
			(HOMO-1)-α → LUMO-α (0.15)

In Table 1, the calculated results for the lowest energy transitions with oscillator strengths larger than the lowest energy transition (0.01) obtained for **1** and **2** at the TD-UCAMB3LYP/6-31G* at optimized ground state geometries are summarized. Results refer to CH_2Cl_2 solutions, but solvent effects are marginal (see SI). Relevant MOs are shown in Figure 11 and a more complete set of frontier MOs can be found in Figure S19.

Both radical dyads show in the 364-375 nm region three transitions mainly localized on the PTM unit with minor contributions from bridge states. These transitions are readily assigned to the strong and structured peak observed at ~385 nm. Several transitions are observed at lower energy for both compounds all showing some IET character, even if a large mixing is observed with excitations involving bridge-state, as expected on physical basis.[52] These transitions are assigned to the many broad features observed in experimental spectra in the low-frequency region. Indeed the relevant energy is overestimated by ~0.6 eV, large errors are expected due to the problems of TD-DFT with CT states and in radical species.[53-55] For comparison, analogous results at the B3LYP level (see SI) underestimate the transitions by a similar amount. The oscillator strength associated with this lowest energy transition is a small fraction (1/50-1/100) of the oscillator strength associated with the intense peak localized on PTM, in line with the experimental data.

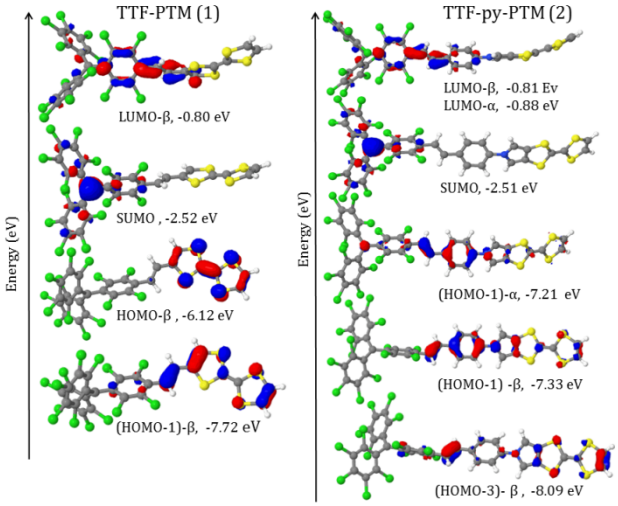

Figure 11. MOs involved in lowest energy transitions (see Table 1).

Calculations on the isolated dyad **2** at the crystallographic geometry support a largely neutral ground state both at room and at low temperature (Table S6), in agreement with experimental data. Quite interestingly the charge separation slightly decreases on molecule A upon decreasing temperature, while for molecule B a larger increase of ionicity is observed, in line with an improved delocalization.

Conclusions

In summary, we have reported the synthesis and characterization of the new donor-acceptor dyad **2**, a

TTF-pyrrolo-annulated-PTM radical, with an extended structure that allowed single crystals of good quality to be obtained. Analysis of the Raman spectra and X-ray bond lengths of the radical dyad **2** and its non-radical counterpart **10** indicates that there is some □-conjugation between the MPTTF donor and the PTM radical acceptor although the dyad is maintained in the neutral state at room temperature. The X-ray structure of **2** revealed a segregation of the donor and acceptor subunits with a regular stacking of the MPTTF along one direction where such units tend to form a *herringbone* arrangement with short (3.85 Å at 150 K) interactions between the S atoms. Interestingly, when decreasing the temperature one of the two non-equivalent molecules (**2B**) becomes much more delocalized, as demonstrated by X-ray bond lengths, whereas the other non-equivalent molecule remains less delocalized (**2A**). In accordance with the original design strategy, the extension of the distance between the MPTTF and PTM moieties has enabled to growth crystals of MPTTF-PTM radical dyad, with a packing in which the donor and the acceptor subunits are segregated and the neighboring MPTTFs show a (modest) degree of interaction. This donor-acceptor radical dyad is the first example of promising molecular building-blocks for the development of novel spintronic molecular materials in view of its solid-state structure and electronic properties.

Experimental Section

General methods: ^{1}H NMR spectra were recorded using a Bruker Avance 250, 400, or 500 instruments and Me_4Si as an internal standard. Infrared spectra were recorded with Spectrum One FT-IR Spectroscopy instrument and UV/Vis/NIR spectra were measured using Cary 5000E Varian. ESR spectra were performed with a Bruker ESP 300 E equipped with a rectangular cavity T102 that works with an X-band (9.5 GHz). The solutions were degassed by argon bubbling before the measurements. LDI/TOF MS were recorded in a Bruker Ultraflex LDI-TOF spectrometer. Cyclic voltammetry measurements were obtained with a potentiostat 263a from EG&G Princeton Applied Research in a standard 3 electrodes cell. The Raman spectra of **1**, **1**$^{+}$·, and **2** are FT–Raman spectra obtained in a Bruker Equinox 55 FT–IR interferometer using a Raman accessory kit (FRA/106–S). A continuous–wave Nd–YAG laser working at 1064 nm was employed for excitation. A germanium detector operating at liquid nitrogen temperature was used. Raman scattering radiation was collected in a back–scattering configuration with a standard spectral resolution of 4 cm^{-1}. 1000-3000 scans were averaged for each spectrum. The Raman spectra of **2** at 120 K have been collected with the Renishaw 1000 microspectro-meter, with 752 nm excitation. The laser power has been kept to the minimum (less than 1 mW at the sample) to avoid sample degradation. The IR-NIR spectra have been collected with a Bruker FT-IR IFS-66 spectrometer equipped with a Hyperion microscope. The spectral resolution is about 2 cm^{-1} for both spectrometers. For the low-temperature spectra, it has been used a Linkam stage. All reagents and solvents employed for the syntheses were of high purity grade and were purchased from Sigma-Aldrich Co., Merck, and SDS. Dry solvents were used in the chemical reactions and in the cyclic voltammetries. The solvents used for optical spectroscopy and ESR measurements were of HPLC grade (ROMIL-SpS). In addition, for cyclic voltammetry experiments, CH_2Cl_2 was filtered over basic alumina to eliminate the acidic residues.

Compound 5: A degassed solution of 1,3-dithiol-2-thione (**3**)[S2] (0.49 g, 3.65 mmol) and 5-tosyl-(1,3)-dithiolo[4,5-*c*]pyrrol-2-one (0.75 g, 2.43 mmol) (**4**) dissolved in freshly distilled $P(OEt)_3$ (30 mL) was heated at 130 °C. After 10 min another portion of **4** (0.49 g, 3.65 mmol, 7.35 eq in total) was added. The reaction mixture was heated for 3 h before being cooled to room temperature. Addition of cold MeOH (50 mL) produced a yellow precipitate, which was filtered and washed with MeOH (3 × 15 mL). The resulting solid was dried and then dissolved in a small portion of CH_2Cl_2 and subjected to purification by flash chromatography (SiO_2, CH_2Cl_2: Petroleum Ether, 1:2, v/v, gradient elution). The yellow band (R_f = 0.6, CH_2Cl_2: Petroleum Ether, 1:1) was collected and the solvent evaporated affording **5** (0.68 g, 71%) as a yellow solid (mp = 250 °C). ^{1}H NMR (400 MHz, CD_3SOCD_3) δ (ppm) = 2.38 (s, 3H, Ts-CH_3), 6.74 (s, 2H, HC=CH), 7.36 (s, 2H, α-H pyrrole), 7.46 (d, 2H, J = 8.2 Hz, Ar-H), 7.83 (d, 2H, J = 8.2 Hz, Ar-H). ^{13}C NMR (100 MHz, CD_3SOCD_3) δ (ppm) = 21.1 (Ts-CH_3), 112.4 (pyrrole α-C), 112.7 (fulvalene C=C), 118.7 (fulvalene C=C), 119.6 (HC=CH), 126.7 (dithiol =C-C=), 126.9 (Ar-C-2), 130.4 (Ar-C-3), 134.5 (Ar-C-1), 145.8 (Ar-C-4). MS (EI): *m/z* (%) = 394.96 [M$^+$, 100]. IR (KBr) □□□(cm^{-1}) = 3137, 1635, 1596, 1370 (SO_2), 1225, 1172 (SO_2), 1090, 1055, 680. CV (n-Bu_4NPF_6 0.1 M in CH_3CN at 298 K vs Ag/AgCl): $E_{1/2}{}^1$ = +0.27 V; $E_{1/2}{}^2$ = +0.49 V. Elemental Analysis: Anal. Calcd. for $C_{15}H_{11}NO_2S_5$: C: 45.31; H: 2.79; N: 3.52. Found: C: 44.82; H: 2.86; N: 3.40.

Compound 6: Compound **5** (0.46 g, 1.15 mmol) was dissolved in a mixture of anhydrous THF - MeOH (1:1, v/v, 24 mL). The solution was degassed for 20 min under Argon atmosphere, whereupon a solution of NaOMe in MeOH (25%, ca 1.4 mL, 1.0 g, 25 mmol) was added in one portion. The mixture was refluxed at 78 °C for 15 min, then cooled to room temperature and concentrated to half volume. Water (50 mL) was added, producing a yellow precipitate, where after the suspension was extracted with CH_2Cl_2 (2 ⍰ 20 mL). The combined organic phases were washed with H_2O (2 ⍰ 20 mL) and brine (2 ⍰ 20 mL) and subsequently dried ($MgSO_4$). After evaporation of the solvent, the green crude product was purified by flash chromatography (SiO_2 deact, CH_2Cl_2). The yellow band (R_f = 0.6, CH_2Cl_2) was collected and the solvent evaporated to afford **6** (0.25 g, 90%) as a yellow powder (mp = 190-191 °C). ^{1}H NMR (500 MHz, $CDCl_3$) δ (ppm) = 6.72 (s, 2H, HC=CH), 6.78 (d, 2H, J = 2.71 Hz, pyrrole α-H), 11.08 (s, 1H, NH). ^{13}CNMR (125 MHz, $CDCl_3$) δ (ppm) = 109.7 (pyrrole α-C), 115.3 (fulvalene C=C), 116.2 (fulvalene C=C), 118.7 (dithiol =C-C=), 120.6 (HC=CH). MS (EI): *m/z* (%) = 243 [M^+, 100]. IR (KBr) ⍰⍰(cm^{-1}) = 3410 (NH stretch), 3124, 1629 (NH), 1531, 1252 (C-N). CV (*n*-Bu_4NPF_6 0.1 M in CH_3CN at 298 K vs Ag/AgCl): $E_{1/2}{}^1$ = +0.37 V; $E_{1/2}{}^2$ = +0.72 V. Elemental Analysis: Anal. Calcd. for $C_6H_5NS_4$: C: 39.48; H: 2.07; N: 5.75. Found: C: 40.18; H: 2.11; N: 5.44.

Compound 8: A Schlenk tube containing a mixture of compound **6** (71 mg, 0.291 mmol), 4-iodobenzaldehyde (**7**) (171 mg, 7.37 mmol), K_3PO_4 (230 mg, 10.8 mmol), and CuI (113 mg, 5.93 mmol) dissolved in freshly distilled THF (5 mL) was degassed under argon for 15 min, where after ±-trans-1,2-diaminocyclohexane (0.1 mL, 0.83 mmol) was added to the solution and the vial capped. The reaction mixture was heated for 3 h at 105 °C, cooled to room temperature and the solution was extracted with CH_2Cl_2 and washed with water (4 ⍰ 20 mL). The combined organic phases were combined, dried ($MgSO_4$) and concentrated to give an orange solid that was purified using flash chromatography (SiO_2, CH_2Cl_2:Toluene, 1:1, v/v). The yellow band (R_f = 0.3, CH_2Cl_2:Toluene, 1:1) was collected and concentrated to provide the desired compound **8** as a red solid (59.7 mg, 59 %). Shiny crystals of **8** were obtained from CH_2Cl_2:Et_2O (1:1). ^{1}H NMR (500 MHz, CD_3SOCD_3) δ (ppm) = 9.98 (s, 1 H, -CHO), 7.94 (d, 2H, J = 8.2 Hz, Ar-H), 7.45 (d, 2H, J = 8.2 Hz, Ar-H), 6.99 (s, 2H, pyrrole α-H), 6.34 (s, 2 H, HC=CH). ^{13}C NMR (125 MHz, CD_3SOCD_3) δ (ppm) = 190.8, 136.2, 131.7, 126.6, 119.7, 119.0, 118.6, 110.1.(2 lines are missing/overlapping). MALDI-MS (DCTB): *m/z* (%) = 347.6 [M^+, 100]. CV (*n*-Bu_4NPF_6 0.1 M in CH_3CN at 298 K): $E_{1/2}{}^1$ = +0.28 V; $E_{1/2}{}^2$ = +0.64 V. Elemental Analysis: Anal. Calcd. for $C_{15}H_9NOS_4$: C: 51.85; H: 2.61; N: 4.03. Found: C: 51.33; H: 2.49; N: 3.65.

Compound 10: The phosphonated PTM derivative **9**[S1] (344 mg, 0.39 mmol) was dissolved in anhydrous THF (60 mL) under strict inert conditions, whereupon the solution was cooled down to -78 ºC. Potassium *tert*-butoxide (98 mg, 0.87 mmol) was added and the reaction mixture was stirred for 20 minutes to form the yellow-orange ylide. Susequently, the MPTTF compound **8** (150 mg, 0.43 mmol) was added and the reaction mixture was allowed to warm up to room temperature. After being stirred for 3 d at room temperature, the reaction mixture was extracted with CH_2Cl_2, washed with H_2O, and dried ($MgSO_4$). The solvents were evaporated and the crude product was purified by column chromatography (SiO_2, Et_2O:hexanes, 1:1, v/v) to provide the desired compound **10** as a light orange powder (290 mg, 69%). ^{1}H NMR (400 MHz, CD_3SOCD_3) δ (ppm) = 7.75 (d, 2H, J = 8.2 Hz, Ar-H), 7,59 (d, 2H, J = 8.2 Hz, Ar-H), 7.53 (s, 2H, pyrrole α-H), 7.22 (d, 1H, J = 16.8 Hz, Phenyl-CH=CH-PTM), 7.13 (d, 1H, J = 16.8 Hz, Phenyl-CH=CH-PTM), 6.95 (s, 1H, ⍰H), 6.76 (s, 2H, HC=CH). FT-IR ⍰⍰(cm^{-1}) = 2955 (w), 2922 (w), 2855 (w), 1728 (w), 1602 (m, CH=CH), 1517 (s), 1487 (m), 1461 (w), 1381 (m), 1370 (m), 1335 (m), 1309 (s), 1185 (m), 1138 (m), 1038 (m), 967 (m), 936 (m), 869 (w), 806 (s), 750 (m), 691 (m). UV-VIS-NIR (CH_2Cl_2, ⍰$_{max}$ (nm), ⍰ in (M^{-1}·cm^{-1})) = 327 (15958); 377 (14848). LDI-TOF (positive mode): *m/z* (amu/e^-): 1069.721 CV (*n*-Bu_4NPF_6 0.1 M in CH_2Cl_2 as electrolyte vs Ag/AgCl): $E_{½}{}^1$ = +0.49 V; $E_{½}{}^2$= + 0.99 V.

Compound 2: Compound **10** (90 mg, 0.08 mmol) was dissolved in distilled CH_2Cl_2 (40 mL) and a solution of *n*-Bu_4NOH (1.0 M in MeOH, 120 ⍰L, 0.12 mmol) was added. The purple reaction mixture was stirred for 4 h before $AgNO_3$ (24 mg, 0.14 mmol) dissolved in acetonitrile (10 mL) was added. The reaction mixture was then stirred for further 90 min and the solution changes color from purple to dark brown and a precipitate of silver (Ag^0) was formed. Subsequently, the reaction mixture solution was filtered and the filtrate concentrated. Finally, the crude product was purified by flash column chromatography (SiO_2, CH_2Cl_2:hexanes, 1:1, v/v) to produce the desired TTF-Pyrrole-Phenyl-PTM radical **2** as a dark reddish-brown powder (64 mg, 71%). FT-IR ⍰⍰(cm^{-1}) = 2952 (m), 2922 (s), 2855 (m), 1727 (w), 1660 (w), 1626 (w), 1605 (m, CH=CH), 1519 (s), 1456 (w), 1427 (w), 1382 (m), 1335

(s), 1311 (s), 1257 (m), 1183 (m), 1155 (w), 1038 (m), 966 (m), 936 (m), 875 (w), 815 (s), 795 (m), 753 (m), 734 (m). UV-VIS-NIR (CH_2Cl_2, λ_{max} (nm), ε ($M^{-1}\cdot cm^{-1}$)) = 199 (13176), 321 (12730), 375 (13207), 386 (16220), 439 (4950). LDI-TOF (positive mode): *m/z* (amu/e^-): 1069.643 $[M]^{+}\cdot$, 997.698 $[M-70]^{+}$, (negative mode): 1069.653 $[M]^{-}\cdot$. CV (*n*-Bu_4NPF_6 0.1 M in CH_2Cl_2 as electrolyte vs Ag/AgCl): $E_{½}^{1}$ = −0.156 V, $E_{½}^{2}$ = +0.471 V, $E_{½}^{3}$ = +0.970. ESR (CH_2Cl_2) *g* = 2.0025.

Acknowledgements

This work was supported by the DGI grant (BeWell; CTQ2013-40480-R), the Networking Research Center on Bioengineering, Biomaterials, and Nanomedicine (CIBER-BBN), and the Generalitat de Catalunya (grant 2014-SGR-17). The work was partly supported by CINECA, through ISCRA-MMM, and by MIUR, through PRIN-2012T9XHH7. M.S. is grateful to MEC for a FPU predoctoral grant. F.D. was partly supported by ERASMUS PLACEMENT CONSORTIA. In Denmark, this work was supported by the European Commission (EC) FP7 Initial Training Networks (ITN) "FUNMOLS" Project No. 212942 and "MOLESCO" Project No. 606728 and the Danish Council for Independent Research | Natural Sciences (#11-106744). We thank Amable Bernabé for MALDI spectroscopy. We thank Vega Lloveras for ESR spectroscopy. We thank Cristina Sissa for useful discussion and help.

Keywords: Donor-acceptor • tetrathiafulvalene • polycholotriohenylmethyl radical • intramolecular charge transfer • self-assembled architecture

[1] F. M. Raymo, *Adv. Mater.* **2002**, *14*, 401-414.

[2] P. Gutlich, A. Hauser, H. Spiering, *Angew. Chem. Int. Ed.* **1994**, *33*, 2024-2054.

[3] O. Sato, J. Tao, Y. Z. Zhang, *Angew. Chem. Int. Ed.* **2007**, *46*, 2152-2187.

[4] I. Ratera, D. Ruiz-Molina, J. Vidal-Gancedo,K. Wurst, N. Daro, J-D. Letard, C. Rovira, J. Veciana, *Angew. Chem. Int. Ed.* **2001**, *40*, 919-922.

[5] I. Ratera, J. Veciana, *Chem. Soc. Rev.* **2012**, *41*, 303.

[6] J. M. Tour, M. Kozaki, J. M. Seminario, *J. Am. Chem. Soc*. **1998**, *120*, 8486.

[7] J.-M. Lehn, *Science* **2002**, *295*, 2400.

[8] Y. Yamamoto, T. Fukushima, Y. Suna, N. Ishii, A. Saeki, S. Seki, S. Tagawa, M. Taniguchi, T. Kawai, T. Aida, *Science* **2006**, *314*, 1761-1764.

[9] E. H. Beckers, S. C. Meskers, A. P. Schenning, Z. Chen, F. Würthner, P. Marsal, D. Beljonne, J. Cornil, R.A. Janssen, *J. Am. Chem. Soc*. **2006**, *128*, 649-657.

[10] N. Kondo, M. Uchikawa, S. Kume, H. Nishihara, *Chem. Commun.* **2009**, 1993-1995.

[11] A. Scott, A. B. Ricks, M. T. Colvin, M. R. Wasielewski, *Angew. Chem. Int. Ed.* **2010**, *49*, 2904-2908.

[12] O. Elsner, D. Ruiz-Molina, J. Vidal-Gancedo, C. Rovira, J. Veciana, *Chem. Commun.* **1999**, 579-580.

[13] O. Elsner, D. Ruiz-Molina, I. Ratera, J. Vidal-Gancedo, C. Rovira, J. Veciana, *J. Organomet. Chem*. **2001**, *251*, 637−639.

[14] I..Ratera, D. Ruiz-Molina, F. Renz, J. Ensling, K. Wurst, C. Rovira, P. Gütlich, J. Veciana, *J. Am. Chem. Soc.* **2003**, *125*, 1462-1463.

[15] C. Sporer, I. Ratera, D. Ruiz-Molina, Y. Zhao, J. Vidal-Gancedo, K. Wurst, P. Jaitner, K. Clays, A. Persoons, C. Rovira, J. Veciana, *Angew. Chem. Int. Ed.* **2004**, *43*, 5266-5268.

[16] I..Ratera, C. Sporer, D. Ruiz-Molina, N. Ventosa, J. Baggerman, A. M. Brouwer, C. Rovira, J. Veciana, *J. Am. Chem. Soc.* **2007**, *129*, 6117-6129.

[17] G. D'Avino, L. Grisanti, J. Guasch, I. Ratera, J. Veciana, A. Painelli, *J. Am. Chem. Soc.* **2008**, *130*, 12064-12072.

[18] J. .Guasch, L. Grisanti, S. Jung, D. Morales, G. D'Avino, M. Souto, X. Fontrodona, A. Painelli, F. Renz, I. Ratera, J. Veciana, *Chem. Mater.* **2013**, *25*, 808–81.

[19] M. González, J. L. Segura, C. Seoane, N. Martín, J. Garín, J. Orduna, R. Alcalá, B. Villacampa, V. Hernández, J. T. López Navarrete, *J. Org. Chem.* **2001**, *66*, 8872-8882.

[20] D. F. Perepichka, M. R. Bryce, E. J. McInnes, J. P. Zhao, *Org. Lett.* **2001**, *3*, 1431-1434.

[21] S. Nishida, Y. Morita, K. Fukui, K. Sato, D. Shiomi, T. Takui, K. Nakasuji, *Angew. Chem. Int. Ed.* **2005**, *44*, 7277-7280.

[22] C. Jia, S. Liu, C. Tanner, C. Leiggener, A. Neels, L. Sanguinet, E. Levillain, S. Leutwyler, A. Hauser, S. Decurtins, *Chem. Eur. J.* **2007**, *13*, 3804-3812.

[23] S. Kato, M. Kivala, W. B. Schweizer, C. Boudon, J. P. Gisselbrecht, F. Diederich, *Chem. Eur. J.* **2009**, *15*, 8687-8691.

[24] F. Otón, V. Lloveras, M. Mas-Torrent, J. Vidal-Gancedo, J. Veciana, C. Rovira, C. *Angew. Chem. Int. Ed.* **2011**, *50*, 10902-10906.

[25] F. Otón, R. Pfattner, E. Pavlica, Y. Olivier, G. Bratina, J. Cornil, J. Puigdollers, R. Alcubilla, X. Fontrodona, M. Mas-Torrent, J. Veciana, C. Rovira, *Cryst. Eng. Comm.* **2011**, *13*, 6597-6600.

[26] F. G. Brunetti, J. L. López, C. Atienza, N. Martín, *J. Mater. Chem.* **2012**, *22*, 4188-4205.

[27] F. Riobé, P. Grosshans, H. Sidorenkova, M. Geoffroy, N. Avarvari, *Chem. Eur. J.* **2009**, *15*, 380-387.

[28] F. Pop, A. Amacher, N. Avarvari, J. Ding, L. M. Daku, A. Hauser, M. Koch, J. Hauser, S. Liu, S. Decurtins, *Chem. Eur. J*. **2013**, *19*, 2504.

[29] Y. Geng, C. Fiolka, K. Krämer, J. Hauser, V. Laukhin, S. Decurtins, S. Liu, *New J. Chem.* **2014**, *38*, 2052-2057.

[30] J. Guasch, L. Grisanti, V. Lloveras, J. Vidal-Gancedo, M. Souto, D. C. Morales, M. Vilaseca, A. Sissa, A. Painelli, I. Ratera, C. Rovira, J. Veciana, *Angew. Chem. Int. Ed*. **2012**, *51*, 11024-11028.

[31] J. Guasch, L. Grisanti, M. Souto, V. Lloveras, J. Vidal-Gancedo, I. Ratera, A. Painelli, C. Rovira, J. Veciana, *J. Am. Chem. Soc.* **2013**, *135*, 6958-6967.

[32] M. Souto, J. Guasch, V. Lloveras, P. Mayorga, J. T. López Navarrete, J. Casado, I. Ratera, C. Rovira, A. Painelli, J. Veciana, *J. Phys. Chem. Lett.* **2013**, *4*, 2721-2726.

[33] M. Souto, D. C. Morales, J. Guasch, I. Ratera, C. Rovira, A. Painelli, J. Veciana, *J. Phys. Org. Chem*. **2014**, *27*, 465-469.

[34] S. Nygaard, C. N. Hansen, J. O. Jeppesen, *J. Org. Chem.* **2007**, *72*, 1617-1626.

[35] J. O. Jeppesen, K. Takimiya, F. Jensen, J. Becher, *Org. Lett.* **1999**, *1*, 1291-1294.

[36] J. O. Jeppesen, K. Takimiya, F. Jensen, T. Brimert, K. Nielsen, N. Thorup, J. Becher, *J. Org. Chem.* **2000**, *65*, 5794-5805.

[37] H. Li, C. Lambert, *Chem. Eur. J.* **2006**, *12*, 1144-1155.

[38] Y. Salinas, M. V. Solano, R. E. Sørensen, K. R. Larsen, J. Lycoops, J. O. Jeppesen, R. Martínez-Máñez, F. Sancenón, M. D. Marcos, P. Amorós, C. Guillem, *Chem. Eur. J.* **2014**, *20*, 855.

[39] M. V. Solano, E. A. D. Pia, M. Jevric, C. Schubert, X. Wang, C. Van der Pol, K. Nørgaard, D. M. Guldi, M. B. Nielsen, J. O. Jeppesen, *Chem. Eur. J.* **2014***, 20,* 9918-9929*.*

[40] C. Rovira, D. Ruiz-Molina, O. Elsner, J. Vidal-Gancedo, J. Bonvoisin, J.-P. Launay, J. Veciana, *Chem. Eur. J.* **2001**, 7, 240-250.

[41] In previous work, see Refs. [30,31], we were not able to observe the IET transition of **1**, since we used slightly acidic solvents such as CH_2Cl_2. Such an IET transition appears as a very weak and broad band if properly treated solvents (fresh distilled and filtered through basic alumina) are used.

[42] V. Mukherjee, N. P. Singh, *Spectrochim. Acta A*, **2014**, *117*, 315-322.

[43] J. Guasch, X. Fontrodona, I. Ratera, C. Rovira, J. Veciana, *Acta. Cryst.*, **2013**, *69*, 255.

[44] A. Girlando, L. Grisanti, M. Masino, I. Bilotti, A. Brillante, R. G. Della Valle, E. Venuti, *Phys. Rev. B* **2010**, *82*, 035208.

[45] S. R. González, B. Nieto-Ortega, R. C. González Cano, V. Lloveras, J. J. Novoa, F. Mota, J. Vidal-Gancedo, C. Rovira, J. Veciana, E. Del Corro, M. Taravillo, V. G. Baonza, J. T. López Navarrete, J. Casado, *J. Chem. Phys.* **2014**, 164903, 1-9.

[46] C. Pecile, A. Painelli, A. Girlando, *Mol. Cryst. Liq. Cryst.* **1989**, *171*, 69-73.

[47] R. Bozio, I. Zanon, A. Girlando, C. Pecile, *J. Chem. Phys.* **1979**, *71*, 1979-1985.

[48] S. Matsuzaki, T. Moriyama, K. Toyoda, **1980**, *34*, 857-859.

[49] S. Matsuzaki, M. Onomichi, H. Tomura, S. Yoshida, K. Toyoda*, Mol. Cryst. Liq. Cryst.* **1985**, *120*, 93-96.

[50] M. J. Frisch, G. W. Trucks, H. B. Schlegel, G. E. Scuseria, M. A. Robb, J. R. Cheeseman, G. Scalmani, V. Barone, B. Mennucci, G. A. Petersson, H. Nakatsuji, M. Caricato, X. Li, H. P. Hratchian, A. F. Izmaylov, J. Bloino, G. Zheng, J. L. Sonnenberg, M. Hada, M. Ehara, K. Toyota, R. Fukuda, J. Hasegawa, M. Ishida,T. Nakajima, Y. Honda, O. Kitao, H. Nakai, T. Vreven, J. A. Montgomery, Jr., J. E. Peralta, F. Ogliaro, M. Bearpark, J. J. Heyd, E.Brothers, K. N. Kudin, V. N. Staroverov, T. Keith, R. Kobayashi,Normand, K. Raghavachari, A. Rendell, J. C. Burant, S. S. Iyengar, J. Tomasi, M. Cossi, N. Rega, J. M. Millam, M. Klene, J. E. Knox, B. Cross, V. Bakken, C. Adamo, J. Jaramillo, R. Gomperts, R. E. Stratmann, O. Yazyev, A. J. Austin, R. Cammi, C. Pomelli, J. W. Ochterski, R. L. Martin, K. Morokuma, V. G. Zakrzewski, G. A. Voth, P. Salvador,

J. J. Dannenberg, S. Dapprich, A. D. Daniels, O. Farkas, J. B. Foresman, J. V. Ortiz, J. Cioslowski, and D. J. Fox, Gaussian, Inc., Wallingford CT, **2010**.

[51] R. Cammi, J. Tomasi, *J. Comput. Chem.* **1995**, *16*, 1449-15458.

[52] L. Grisanti, G. F'Avino, A. Painelli, J. Guasch, I. Ratera, J. Veciana, *J. Phys. Chem. B.* **2009**, *113*, 4718-4725.

[53] A. Ipatov, F. Cordova, L. J. Doriol, M. Casida, *J. Molec. Struct., TEOCHEM* **2009**, *914*, 60-73

[54] A. Dreuw, M. Head-Gordon, *Chem. Rev*. **2005**, *105*, 4009-4039, and references cited therein.

[55] C. Adamo, D. Jacquemin, *Chem. Soc. Rev*. **2013**, *42*, 845-856.

Entry for the Table of Contents

An electron donor-acceptor dyad based on a polychlorotriphenylmethyl (PTM) radical subunit linked to a tetrathiafulvalene (TTF) unit through a π-conjugated *N*-phenyl-pyrrole-vinylene bridge has been synthesized and characterized. The intramolecular electron transfer (IET) process and magnetic properties of the radical dyad have been evaluated by cyclic voltammetry, UV-Vis, vibrational, and ESR spectroscopies both in solution and in the solid state. The self-assembling ability of the radical dyad and of its protonated non-radical analogue has been investigated by X-ray crystallographic analysis which reveals that the radical dyad produces a supramolecular architecture with segregated donor and acceptor units where the TTF subunits are arranged in 1-D herringbone type stacks. Analysis of the X-ray data at different temperatures suggests that the two non-equivalent molecules that form the asymmetric unit of the crystal of the radical dyad evolve into an opposite degree of electronic delocalization as the temperature decrease.

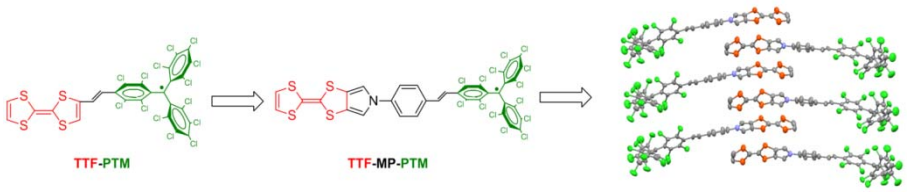

*Manuel Souto, Marta V. Solano, Imma Ratera, Morten Jensen, Dan Bendixen, Francesca Delchiaro, Alberto Girlando, Anna Painelli, Jan O. Jeppesen, Concepció Rovira,Jaume Veciana**

Self-assembled architectures with segregated donor and acceptor units of a dyad based on a monopyrrolo-annulated TTF-PTM radical